Localization Transition for Interacting Quantum Particles in Colored-Noise Disorder

Giacomo Morpurgo,[1,2,3] Laurent Sanchez-Palencia,[4] and Thierry Giamarchi[1]
[1]Department of Quantum Matter Physics, University of Geneva, 1205 Geneva, Switzerland
[2]International Solvay Institutes, 1050 Brussels, Belgium
[3]Center for Nonlinear Phenomena and Complex Systems, Université libre de Bruxelles, CP 231, Campus Plane, B-1050 Brussels, Belgium
[4]CPHT, CNRS, Ecole Polytechnique, IP Paris, F-91128 Palaiseau, France

(Received 28 July 2025; revised 19 December 2025; accepted 9 February 2026; published 4 March 2026)

We investigate the localization transition of interacting particles in a one-dimensional system with colored-noise disorder, where backward scattering processes are suppressed beyond a cutoff. Employing two complementary renormalization group procedures, we derive the phase diagram and reveal a significant shift in the localization transition point, governed by correlations. Our numerical analysis further demonstrates that the scaling of the localization length with disorder strength deviates markedly from the conventional behavior observed in typical localized phases, highlighting the unique impact of correlated disorder on interacting quantum systems. Application to optical disorder used in cold atom experiments is discussed.

DOI: 10.1103/c81j-h58j

The discovery of Anderson localization (AL) [1] has unveiled the profound impact of disorder on the electronic properties of noninteracting materials, sparking extensive investigations into disorder effects within quantum systems. This impact is particularly pronounced in low-dimensional systems, where even an infinitesimal amount of disorder can fundamentally alter the nature of electronic wave functions, resulting in localization. A major challenge in this domain is elucidating the interplay between disorder and interactions [2–4]. The most striking manifestations of this interplay are observed in low-dimensional systems, where both interaction effects [5] and disorder are maximal. This confluence gives rise to a plethora of novel phenomena, including the emergence of Bose glass phases [6,7] and many-body localization [8–10].

To date, investigations have predominantly focused on white-noise disorder. However, experimental realizations typically exhibit finite spatial correlations, thus constituting so-called colored-noise disorder. Such correlations can significantly influence the behavior of diverse systems, ranging from crystallography to superconductivity and AL [11–13]. This has spurred a substantial amount of theoretical and experimental research within quantum simulation platforms, such as ultracold atom and cavity polariton systems, where disorder correlations are well characterized and can be engineered. For instance, extensive studies have been conducted on quasiperiodic models both with and without interactions [14–24]. In contrast, truly disordered systems with finite correlations have received less attention. A simple model that captures colored-noise correlations involves decreasing Fourier components with a cutoff. Owing to fundamental optical constraints, this approach is precisely what is achieved in speckle potentials within cold atomic systems [25–29]. In 1D systems, suppression of backscattering beyond the cutoff effectively suppresses single-particle AL, leading to the appearance of a pseudomobility edge where the localization length varies by orders of magnitude [30]. This phenomenon can be harnessed to control AL through correlation engineering in such potentials [31,32]. Additionally, studies have explored AL of collective excitations in weakly interacting 1D bosons within Bogoliubov formalism [33–36]. In contrast, the impact of colored-noise disorder correlations on the localization of quantum particles in the strongly interacting regime remains unexplored.

In this Letter, we show that an interacting 1D quantum system transitions from localization to delocalization under colored-noise disorder with a momentum cutoff. Using universal Tomonaga-Luttinger liquid (TLL) theory, we address both bosons and fermions within a unified framework. Our most significant finding reveals that, at the cutoff, the critical properties of the localization-delocalization transition are profoundly altered compared to those observed with standard white-noise disorder. Renormalization group (RG) analysis indicates a shift in the critical point from the Luttinger parameter $K^* = 3/2$ (white noise) to $K^* = 1$ (colored noise) in the weak-disorder and Gaussian-correlated regime. This result is corroborated through direct perturbative RG analysis of a microscopic interacting Fermi model. Additionally, we observe an unusual scaling of the localization length with disorder strength. Our results reveal the substantial impact of spatial disorder correlations on the critical properties of interacting quantum systems, with direct implications for

speckle potentials and other forms of colored-noise disorder implementable via digital mirror devices (DMDs).

Using the bosonized representation [5,37], which describes well the low-energy properties of the system, the Hamiltonian reads

$$H = H_0 + H_W, \tag{1}$$

$$H_0 = \frac{1}{2\pi}\int dx\, u\left[K\big(\nabla\theta(x,\tau)\big)^2 + \frac{1}{K}\big(\nabla\phi(x,\tau)\big)^2\right], \tag{2}$$

$$H_W = \frac{1}{\pi\alpha}\int dx\, W(x)\cos\big(2\phi(x) - 2k_{\mathrm{F}}x\big), \tag{3}$$

where ϕ and θ are two bosonic fields with the commutation relation $[(1/\pi)\nabla\phi(x), \theta(x')] = -i\delta(x-x')$, u is the speed of sound, and K is the dimensionless (interaction-dependent) Luttinger parameter. This representation applies to fermionic, bosonic, or spin systems both in the continuum and in a lattice. The quantity $k_{\mathrm{F}} = \pi\rho_0$, with ρ_0 being the average density, is the Fermi wave vector, and α is an ultraviolet cutoff of the order of the lattice spacing for a lattice model. For fermionic systems, $K = 1$ corresponds to free fermions, while $K > 1$ ($K < 1$) corresponds to attractive (repulsive) interactions. For bosonic systems with contact-repulsive interactions, $K \in [1, \infty[$, with $K = 1$ corresponding to infinite repulsion (Tonks limit) and $K \to +\infty$ to free bosons [5,38].

The term H_W represents the backscattering of particles with momentum close to k_{F} (scattering with transfer momentum $2k_{\mathrm{F}}$) from a disorder potential $W(x)$, as shown in Fig. 1(a). In 1D, the forward and backward scatterings can be decoupled [6]. Since only the backscattering affects the current, we neglect the forward component of the disorder in this Letter (see the Supplemental Material [39] for more details on the forward scattering).

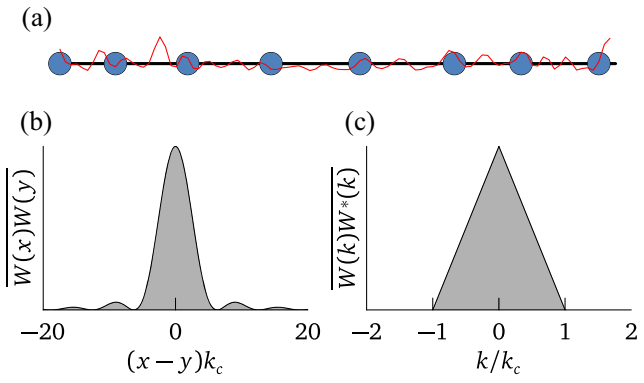

FIG. 1. Sketch of a colored-noise disorder as considered in this Letter. (a) Realization of a 1D speckle potential (red line) with quantum particles (blue disks). (b) Two-point correlation function of a speckle potential in real space. (c) Two-point correlation function of a speckle potential in momentum space. The latter has a triangular form with a high-momentum cutoff at $|k| = k_c$.

We consider a colored-noise disorder that can potentially make the backscattering vanish. One example is the speckle disorder (SD) [40,41], which has been instrumental in observing single-particle AL in cold atomic gases [26,42,43]. It stems from the square of a random, Gaussian-correlated, complex field, so that it is non-Gaussian and nonsymmetric. Its two-point spatial correlation function is a squared sinc function; see Fig. 1(b). The speckle disorder has finite momentum support, such that the second moment of the correlations of the potential vanishes above a momentum cutoff k_c; see Fig. 1(c). It can be either repulsive (blue-detuned, BSD) or attractive (red-detuned, RSD). In order to disentangle some of the effects due to the colored noise from the existence of odd moments for BSD and RSD due to their non-Gaussian character, we also study a Gaussian, colored disorder (GCD) with the same correlation function. In both cases, the second moment reads

$$\overline{W_k W_{-k'}} = W_0^2(1 - |k|/k_c)\theta(k_c - |k|)\Omega\delta_{k,k'}, \tag{4}$$

where the overbar denotes the average over disorder realizations, W_0 is the disorder intensity, Ω is the volume of the system, and $\delta_{k,k'}$ is the Kronecker delta. Note that the factor Ω comes from the use of discrete values of k, and the spatial correlations do not depend on the volume of the system. More details can be found in the Supplemental Material [39].

To consider the combined effects of disorder and interactions, we treat the disorder term in Eq. (1) using a perturbative RG procedure. Working along the lines of Ref. [18], we integrate the short-distance properties by increasing the cutoff $\alpha(l) = \alpha e^l$. This is equivalent to integrating the momenta in a shell around $2k_{\mathrm{F}}$ with width $1/\alpha(l)$. It yields the RG equations [39]

$$\frac{\partial K}{\partial l} = -\frac{K^2 y^2}{2}\frac{1}{\Omega}\sum_k\left(1 - \frac{|k|}{k_c}\right)\theta(k_c - |k|) \times \left[J_0\big((k + 2k_{\mathrm{F}})\alpha(l)\big) + J_0\big((k - 2k_{\mathrm{F}})\alpha(l)\big)\right], \tag{5}$$

$$\frac{\partial y^2}{\partial l} = (4 - 2K)y^2, \tag{6}$$

where $y = (\alpha W_0/u)$, and J_0 is the Bessel function. The latter acts as a "window" filtering the modes far from the Fermi wave vector by a value of order $1/\alpha(l)$. At this order, the RG equations depend only on the second moment of the disorder correlations, and they are thus identical for SD and GCD. The appearance of the Bessel functions is due to our choice of a hard cutoff in real space and, similarly to Ref. [18], we replace them with windows $[J_0(q\alpha) \to \theta(1 - |q|\alpha)]$ centered at $2k_{\mathrm{F}}$ or $-2k_{\mathrm{F}}$. Intuitively, the RG procedure amounts to making these windows narrower and narrower, thus capturing only the physics which occurs there at low energy (i.e., at $\sim \pm 2k_{\mathrm{F}}$).

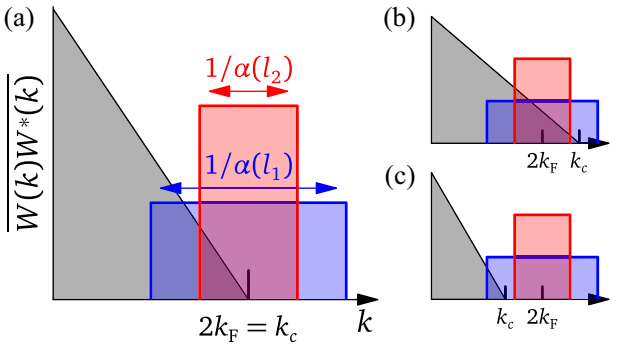

FIG. 2. Bosonized RG procedure: As $\alpha(l)$ increases ($l_1 < l_2$), the windows around $2k_F$ shrink, capturing only the low-energy physics. (a) Case $k_c = 2k_F$. The weight of the disorder in this window becomes vanishingly small as α increases. (b) Case $k_c > 2k_F$. As α increases, there is always a finite weight of the disorder in the shrinking window. We recover the physics of an uncorrelated Gaussian disorder. (c) Case $k_c < 2k_F$. There is a certain l^* after which there is not any weight of the disorder inside the shrinking window. We recover the physics of nondisordered systems.

Three cases of interest arise depending on the value of k_c compared to the Fermi level. For $k_c < 2k_F$, there is a scale l^*, such that $\alpha(l > l^*) > 1/(2k_F - k_c)$ and the window does not contain any disorder anymore, owing to the finite support of the latter; see Fig. 2(c). Hence, no backscattering occurs at this order in the RG, which implies the suppression of localization. Note that higher-order perturbation terms in the disorder may induce backscattering [30]. However, for the case of weak disorder that we consider here, such terms corresponding to a higher power of the disorder would be extremely small and lead potentially only to a huge localization length.

For $k_c > 2k_F$, backscattering is always present at all scales. For $\alpha(l) \gg 1/(k_c - 2k_F)$, the second moment of the disorder is almost constant within the window—see Fig. 2(b)—and we recover the same RG equations as for an uncorrelated Gaussian disorder [6,18]. In that case, the momentum cutoff in the spectrum of the disorder is irrelevant, and we find a localization-delocalization transition (for weak disorder) at the usual critical point $K^* = 3/2$.

The most interesting case, and the central point of our Letter, corresponds to $k_c = 2k_F$, for which backscattering is vanishingly allowed at all scales; see Fig. 2(a). In this case, as we progress in the RG, the window shrinking around $2k_F$ always contains disorder, but with a smaller and smaller weight. The linear decrease of the spectral weight $\overline{W_k W_{-k'}}$ implies that the sum over k in Eq. (5) scales quadratically with $\alpha(l)$, which yields $\partial K/\partial l \propto -y^2/\alpha^2(l)$. Introducing $\tilde{y} = y/\alpha(l)$, we then find the RG equations

$$\frac{\partial K}{\partial l} = -\frac{K^2}{4\pi k_c}\tilde{y}^2, \tag{7}$$

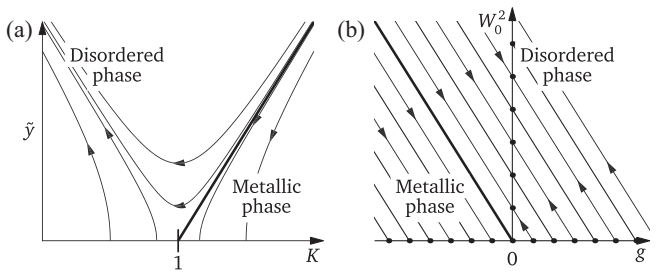

FIG. 3. Phase diagrams. (a) Sketch of the phase diagram versus the Luttinger parameter and renormalized disorder strength, with flow lines from the bosonized RG procedure for $k_c = 2k_F$. The separatrix (bold line) separates the disordered (localized) and metallic (delocalized) phases, with the critical point at K^* in the weak-disorder limit. (b) Sketch of the phase diagram versus interaction and disorder strengths, with flow lines from the diagrammatic RG procedure around the noninteracting Fermi point. Here, the flow is made of straight lines, and we have a line of fixed points in the absence of interactions ($g = 0$).

$$\frac{\partial \tilde{y}}{\partial l} = (1 - K)\tilde{y}. \tag{8}$$

The corresponding RG flow is shown in Fig. 3(a). It shows that in this case, the critical point is at $K^* = 1$, instead of the value $K^* = 3/2$ for white-noise disorder. Hence, for $K < 1$, any arbitrary weak disorder implies localization (disordered phase). Instead, for $K > 1$, we find a localization transition where a finite amount of disorder is necessary to localize, while too-weak disorder implies delocalization (metallic phase). The shift of the critical point implies that a colored noise having backscattering vanishing linearly at $2k_F$ can dominate only for significantly less attractive interactions for fermions (and therefore, more repulsive interactions for bosons) than for standard white-noise disorder. This remarkable shift of the transition point is consistent with the intuitive fact that the backscattering at exactly $2k_F$ would be zero for such a disorder. Nevertheless, due to backscattering at finite momenta around $2k_F$, interactions restore localization at $2k_F$. Note that the value of K^* directly relies on the scaling of the disorder correlation functions at the cutoff k_c. For correlations behaving as $[1 - (|k|/k_c)]^\nu$, following the same steps, we obtain a transition point at $K^* = [(3 - \nu)/2]$. We thus recover the two limit cases: For $\nu = 0$ (white-noise disorder or colored-noise disorder with $2k_F < k_c$), $K^* = 3/2$. For $\nu = 1$ (colored-noise disorder with $2k_F = k_c$), $K^* = 1$. A colored-noise disorder with $0 < \nu < 1$ may be realized using a mask with varying transmission for SD [31,32] or directly engineered using DMDs in cold atom experiments. More details on the derivation of the RG equations and their generalization to $\nu \neq 1$ can be found in the Supplemental Material [39] (specificities linked to the colored disorder) and in Ref. [18] (core idea).

The linear vanishing of the spectral weight of the disorder for standard SD has the advantage to bring back the transition around the noninteracting point for fermions ($K = 1$). This allows us to perform a perturbative RG analysis directly on the microscopic model. Moreover, it avoids the necessity to carefully distinguish elastic and inelastic processes around the noninteracting point in the bosonization procedure [6], which is something highly nontrivial for the correlated disorder discussed here. To proceed, we consider the Fermi Hamiltonian

$$H = \sum_r \sum_k v_F(\varepsilon_r k - k_F) c^\dagger_{r,k} c_{r,k} + \frac{g}{2\Omega} \sum_r \sum_{k,k',q} c^\dagger_{r,k+q} c^\dagger_{-r,k'-q} c_{-r,k'} c_{r,k} + \frac{1}{\Omega} \sum_{k,q\sim 0} \left[W_{q-2k_F} c^\dagger_{R,k+q} c_{L,k} + W_{q+2k_F} c^\dagger_{L,k+q} c_{R,k} \right], \quad (9)$$

where the kinetic term is linearized around the Fermi momentum, v_F is the Fermi velocity, g is the strength of the interactions, $\varepsilon_r = \pm 1$ for respectively right and left movers, and W_{q-2k_F} is defined as before in Eq. (4). We impose an ultraviolet cutoff in momentum space $\Lambda \sim (1/\alpha)$, equivalent to the one used in bosonization. We expand up to second order in interactions g and disorder lines W_0^2, and we look for the second-order diagrams which renormalize the first-order interaction and backscattering diagrams. In both cases, there is a single gW_0^2 diagram to be computed. We find that both second-order diagrams diverge logarithmically with Λ. More details on the procedure [44,45] can be found in the Supplemental Material [39]. Upon varying the cutoff as $\Lambda(l) = \Lambda e^{-l}$, we find the RG equations

$$\frac{\partial g}{\partial l} = -\frac{g W_0^2}{2\pi k_c v_F^2}, \quad (10)$$

$$\frac{\partial W_0^2}{\partial l} = \frac{g W_0^2}{2\pi v_F}. \quad (11)$$

These equations describe a flow that follows straight lines in the g-W_0^2 parameter space; see Fig. 3(b). This flow confirms the predictions of the bosonization approach. For attractive interactions, $g < 0$, the flow reduces the disorder strength. There is a separatrix between the delocalized (metallic) phase, where the disorder fully vanishes, and the localized (disordered) phase, where it grows up to a finite value through RG. Remarkably, we find that the noninteracting line is a line of stable fixed points where the amplitude of the disorder remains constant under the RG flow.

Besides the phase diagrams shown in Fig. 3, computing physical properties, such as the nature of the metallic and disordered phases and transport properties, is challenging. For the phase where the disorder is relevant, higher-order disorder correlations must in principle be taken into account, which we leave for future studies. For the metallic phase, one recovers in principle TLL behavior, characterized by power-law decaying correlation functions and dominant superconducting or superfluid quasi-long-range order. However, this is justified for a disorder with strictly no Fourier component beyond $2k_F$. Higher terms in the disorder—for instance, combining the backward scattering with one forward scattering may generate such Fourier components at order W_0^4, restoring a strict critical point at $K^* = 3/2$. Nevertheless, for $1 < K < 3/2$, the localization length would be extremely large and, far from the critical point, of the order of $\xi \sim (1/D)^{2/(3-2K)}$ with $D = \overline{W(x)W(x)}$. Below such a length, the system would be fully controlled by the colored part of the disorder with its own "localization"-delocalization transition at $K^* = 1$.

To further analyze the consequences of the presence or not of higher moments in the disorder, we may again take advantage of the fact that the noninteracting line is a fixed line by RG in the disordered phase, and consider noninteracting spinless fermions with the tight-binding Hamiltonian

$$H = -t \sum_{\langle i,j \rangle} c^\dagger_i c_j + \text{H.c.} + \sum_i W_i c^\dagger_i c_i, \quad (12)$$

where t is the hopping amplitude, W_i is the disorder potential at site i, and $\Omega = Na$, with a being the lattice spacing, and N the number of sites. We solve the Hamiltonian in Eq. (12) by exact numerical diagonalization, which therefore contains all scattering orders and includes all forward and backward scattering processes. We use a system of 10000 sites for all strengths of disorder. To disentangle the roles of the non-Gaussian character of speckles, their nonsymmetric property, and the existence of a spectral cutoff, we consider BSD, RSD, and GCD. In order to compare to uncorrelated Gaussian disorder (white noise), it is convenient in this section to characterize the disorder strength by its zero-distance correlations $D = \overline{W(x)W(x)} = (W_0^2 k_c/2\pi)$. We set the disorder cutoff to be $k_c = (\pi/2a)$. To extract the localization length ξ of the different eigenstates, we compute the corresponding inverse participation ratio, $\text{IPR} = \int dx |\psi(x)|^4$, and average it over 1000 realizations of the disorder. For weak disorder, the IPR is related to the inverse of the localization length via $\text{IPR} = (1/2\xi)$. The results for $k_F = k_c/2$ are shown in Fig. 4 for BSD, RSD, and GCD. More details on the generation of each type of disorder, the average over the disorder realizations, effects of different system sizes N, as well as numerical results for other values of k_c are given in the Supplemental Material [39]. In particular, for $k_c < 2k_F$, we find ξ of the order of the system size, consistently with effective delocalization.

For $k_c = 2k_F$, the three types of disorder exhibit clear differences showing the role of non-Gaussianity and the presence of higher moments for BSD and RSD.

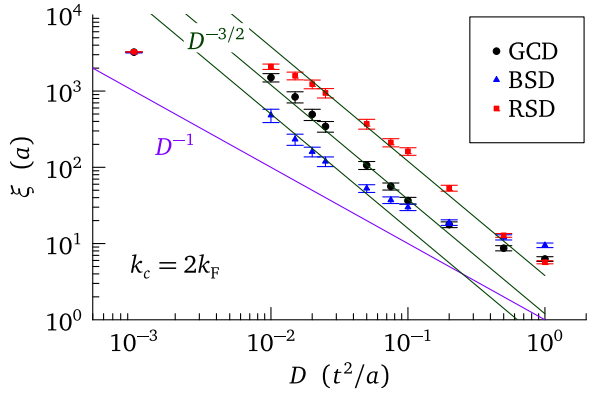

FIG. 4. Localization length ξ versus disorder strength D of the eigenstates of a noninteracting system at momentum $k_F = k_c/2$ for GCD (black circles), BSD (blue triangles), and RSD (red squares). The error bars indicate the standard deviation from disorder averaging (1000 realizations). Guides to the eye of $D^{-3/2}$ behavior for the three sets of data are shown as solid green lines, while the scaling D^{-1} expected for white-noise disorder is shown as a solid purple line for reference. The available range for ξ is limited on one side by the system size ($L/a = 10000$) and on the other side by the reaching of the strong-disorder regime, where usual scalings break down.

The difference between BSD and RSD may be attributed to odd-order disorder terms, which affect localization with opposite contributions [30,46], while GCD has no such terms. In all cases, clear deviations from the usual $1/D$ white-noise behavior are found, showing the role of the vanishing spectral weight of the disorder at $k_c = 2k_F$. As discussed above, higher-order terms in the disorder are expected to give a nonvanishing spectral weight of the disorder at $2k_F$, and thus, to a large but finite localization length. However, such terms are expected to give at least a $1/D^2$ behavior (note that third-order terms in SD have the same threshold at k_c as the second-order term), and none of the three disorders is apparently compatible with that scaling. For GCD and RSD, a scaling compatible with $D^{-3/2}$ is visible in the weak-disorder range and before the localization length is limited by finite-size effects. The precise dependence for BSD is more difficult to ascertain owing to the limited range of the data, but it also seems to show a crossover toward $D^{-3/2}$ at weak disorder. The origin of such a $D^{-3/2}$ scaling is not understood at the moment and is clearly an important target for more numerical investigations and further studies.

In summary, we have investigated the localization of interacting 1D quantum particles, both bosons and fermions, subjected to colored-noise disorder characterized by a vanishing Fourier spectrum. Such correlations are directly inspired by and generalize those inherent in speckle disorder. Our findings demonstrate that in the regime of weak disorder, they significantly modify the critical point for the localization-delocalization transition, a phenomenon governed by disorder correlations. Treating the non-Gaussianities of the speckle disorder by looking at higher-order processes would restore Anderson localization, as shown in Ref. [30], but with localization lengths larger by several orders of magnitude. We analyzed the behavior of the localization length for fermions along the RG fixed line (noninteracting fermions), revealing an unexpected scaling $1/D^{3/2}$ as a function of the disorder strength D. A deeper understanding and further exploration of the properties of such colored-noise disorder presents a significant challenge. On the theoretical front, additional analysis for the noninteracting case is clearly required. For the interacting case, despite the limitations to shorter systems, tensor network or Monte Carlo calculations should allow for a detailed study of the phase diagram and the transition-point shift. Experimentally, true speckle potentials, as well as those generated by digital mirror devices (DMDs), which could implement both GCD and SD, hold promise for observing disorder-induced localization for interacting quantum particles. Since state-of-the-art experimental setups can explore regimes with $k_c/2k_F$ ranging from 0.1 to 2.5, including the ratio $k_c/2k_F = 1$, they should enable accurate probing of the effects studied herein.

Acknowledgments—This work was supported by the Swiss National Science Foundation under Division II (Grant No. 200020-219400); the Agence Nationale de la Recherche under projects QuanTEdu-France (No. ANR-CMAQ-002 France 2030); and QUTISYM (No. ANR-23-PETQ-0002), GENCI-TGCC (Grant No. 2023-A0110510300), and the ERC Grant LATIS.

Data availability—The data that support the findings of this article are openly available [47].

[1] P. W. Anderson, Absence of diffusion in certain random lattices, Phys. Rev. **109**, 1492 (1958).
[2] B. L. Altshuler, A. G. Aronov, and P. A. Lee, Interaction effects in disordered Fermi systems in two dimensions, Phys. Rev. Lett. **44**, 1288 (1980).
[3] A. M. Finkel'stein, Weak localization and Coulomb interaction in disordered systems, Z. Phys. B Conens. Mat. **56**, 189 (1984).
[4] P. A. Lee and T. V. Ramakrishnan, Disordered electronic systems, Rev. Mod. Phys. **57**, 287 (1985).
[5] T. Giamarchi, *Quantum Physics in One Dimension*, International Series of Monographs on Physics Vol. 121 (Oxford University Press, Oxford, 2004).
[6] T. Giamarchi and H. J. Schulz, Anderson localization and interactions in one-dimensional metals, Phys. Rev. B **37**, 325 (1988).
[7] Matthew P. A. Fisher, P. B. Weichman, G. Grinstein, and D. S. Fisher, Boson localization and the superfluid-insulator transition, Phys. Rev. B **40**, 546 (1989).

[8] D. A. Abanin, E. Altman, I. Bloch, and M. Serbyn, Colloquium: Many-body localization, thermalization, and entanglement, Rev. Mod. Phys. **91**, 021001 (2019).
[9] D. J. Luitz, N. Laflorencie, and F. Alet, Many-body localization edge in the random-field Heisenberg chain, Phys. Rev. B **91**, 081103(R) (2015).
[10] J. Z. Imbrie, On many-body localization for quantum spin chains, J. Stat. Phys. **163**, 998 (2016).
[11] D. A. Keen and A. L. Goodwin, The crystallography of correlated disorder, Nature (London) **521**, 303 (2015).
[12] V. D. Neverov, A. E. Lukyanov, A. V. Krasavin, A. Vagov, and M. D. Croitoru, Correlated disorder as a way towards robust superconductivity, Commun. Phys. **5**, 177 (2022).
[13] L. Sanchez-Palencia and M. Lewenstein, Disordered quantum gases under control, Nat. Phys. **6**, 87 (2010).
[14] G. Roati, C. D'Errico, L. Fallani, M. Fattori, C. Fort, M. Zaccanti, G. Modugno, M. Modugno, and M. Inguscio, Anderson localization of a non-interacting Bose-Einstein condensate, Nature (London) **453**, 895 (2008).
[15] D. Tanese, E. Gurevich, F. Baboux, T. Jacqmin, A. Lemaître, E. Galopin, I. Sagnes, A. Amo, J. Bloch, and E. Akkermans, Fractal energy spectrum of a polariton gas in a Fibonacci quasiperiodic potential, Phys. Rev. Lett. **112**, 146404 (2014).
[16] S. Aubry and G. André, Analyticity breaking and Anderson localization in incommensurate lattices, Ann. Isr. Phys. Soc. **3**, 133 (1980).
[17] J. Vidal, D. Mouhanna, and T. Giamarchi, Correlated fermions in a one-dimensional quasiperiodic potential, Phys. Rev. Lett. **83**, 3908 (1999).
[18] J. Vidal, D. Mouhanna, and T. Giamarchi, Interacting fermions in self-similar potentials, Phys. Rev. B **65**, 014201 (2001).
[19] G. Roux, T. Barthel, I. P. McCulloch, C. Kollath, U. Schollwöck, and T. Giamarchi, Quasiperiodic Bose-Hubbard model and localization in one-dimensional cold atomic gases, Phys. Rev. A **78**, 023628 (2008).
[20] C. D'Errico, E. Lucioni, L. Tanzi, L. Gori, G. Roux, I. P. McCulloch, T. Giamarchi, M. Inguscio, and G. Modugno, Observation of a disordered bosonic insulator from weak to strong interactions, Phys. Rev. Lett. **113**, 095301 (2014).
[21] L. Gori, T. Barthel, A. Kumar, E. Lucioni, L. Tanzi, M. Inguscio, G. Modugno, T. Giamarchi, C. D'Errico, and G. Roux, Finite-temperature effects on interacting bosonic one-dimensional systems in disordered lattices, Phys. Rev. A **93**, 033650 (2016).
[22] H. Yao, A. Khoudli, L. Bresque, and L. Sanchez-Palencia, Critical behavior and fractality in shallow one-dimensional quasiperiodic potentials, Phys. Rev. Lett. **123**, 070405 (2019).
[23] H. Yao, T. Giamarchi, and L. Sanchez-Palencia, Lieb-Liniger bosons in a shallow quasiperiodic potential: Bose glass phase and fractal Mott lobes, Phys. Rev. Lett. **125**, 060401 (2020).
[24] M. Schreiber, S. S. Hodgman, P. Bordia, H. P. Lüschen, M. H. Fischer, R. Vosk, E. Altman, U. Schneider, and I. Bloch, Observation of many-body localization of interacting fermions in a quasirandom optical lattice, Science **349**, 842 (2015).
[25] L. Sanchez-Palencia, D. Clément, P. Lugan, P. Bouyer, G. V. Shlyapnikov, and A. Aspect, Anderson localization of expanding Bose-Einstein condensates in random potentials, Phys. Rev. Lett. **98**, 210401 (2007).
[26] J. Billy, V. Josse, Z. Zuo, A. Bernard, B. Hambrecht, P. Lugan, D. Clement, L. Sanchez-Palencia, P. Bouyer, and A. Aspect, Direct observation of Anderson localization of matter waves in a controlled disorder, Nature (London) **453**, 891 (2008).
[27] R. C. Kuhn, C. Miniatura, D. Delande, O. Sigwarth, and C. A. Müller, Localization of matter waves in two-dimensional disordered optical potentials, Phys. Rev. Lett. **95**, 250403 (2005).
[28] R. C. Kuhn, O. Sigwarth, C. Miniatura, D. Delande, and C. A. Müller, Coherent matter wave transport in speckle potentials, New J. Phys. **9**, 161 (2007).
[29] M. Piraud, L. Pezzé, and L. Sanchez-Palencia, Matter wave transport and Anderson localization in anisotropic three-dimensional disorder, Europhys. Lett. **99**, 50003 (2012).
[30] P. Lugan, A. Aspect, L. Sanchez-Palencia, D. Delande, B. Grémaud, C. A. Müller, and C. Miniatura, One-dimensional Anderson localization in certain correlated random potentials, Phys. Rev. A **80**, 023605 (2009).
[31] M. Piraud, A. Aspect, and L. Sanchez-Palencia, Anderson localization of matter waves in tailored disordered potentials, Phys. Rev. A **85**, 063611 (2012).
[32] M. Piraud and L. Sanchez-Palencia, Tailoring Anderson localization by disorder correlations in 1D speckle potentials, Eur. Phys. J. Special Topics **217**, 91 (2013).
[33] V. Gurarie and J. T. Chalker, Some generic aspects of bosonic excitations in disordered systems, Phys. Rev. Lett. **89**, 136801 (2002).
[34] V. Gurarie and J. T. Chalker, Bosonic excitations in random media, Phys. Rev. B **68**, 134207 (2003).
[35] P. Lugan, D. Clément, P. Bouyer, A. Aspect, and L. Sanchez-Palencia, Anderson localization of Bogolyubov quasiparticles in interacting Bose-Einstein condensates, Phys. Rev. Lett. **99**, 180402 (2007).
[36] P. Lugan and L. Sanchez-Palencia, Localization of Bogoliubov quasiparticles in interacting Bose gases with correlated disorder, Phys. Rev. A **84**, 013612 (2011).
[37] F. D. M. Haldane, Luttinger liquid theory of one-dimensional quantum fluids: I. Properties of the Luttinger model and their extension to the general 1D interacting spinless Fermi gas, J. Phys. C Solid State **14**, 2585 (1981).
[38] M. A. Cazalilla, R. Citro, T. Giamarchi, E. Orignac, and M. Rigol, One dimensional bosons: From condensed matter systems to ultracold gases, Rev. Mod. Phys. **83**, 1405 (2011).
[39] See Supplemental Material http://link.aps.org/supplemental/10.1103/c81j-h58jfor further details about the speckle and Gaussian disorder, the effect of forward scattering, details on the derivations of the RG equations, details on the numerical realization of a speckle disorder and numerical results.
[40] J. C. Dainty, *Laser Speckle and Related Phenomena* (Springer science & business Media, New York, 2013), Vol. 9.
[41] J. W. Goodman, *Statistical Optics* (John Wiley & Sons, New York, 2015).

[42] S. S. Kondov, W. R. McGehee, J. J. Zirbel, and B. DeMarco, Three-dimensional Anderson localization of ultracold matter, Science **334**, 66 (2011).

[43] F. Jendrzejeweski, A. Bernard, K. Müller, P. Cheinet, V. Josse, M. Piraud, L. Pezzé, L. Sanchez-Palencia, A. Aspect, and P. Bouyer, Three-dimensional localization of ultracold atoms in an optical disordered potential, Nat. Phys. **8**, 398 (2012).

[44] G. Mahan, *Many-Particle Physics* (Springer, New York, 2000).

[45] J. Sólyom, The Fermi gas model of one-dimensional conductors, Adv. Phys. **28**, 201 (1979).

[46] M. Piraud, P. Lugan, P. Bouyer, A. Aspect, and L. Sanchez-Palencia, Localization of a matter wave packet in a disordered potential, Phys. Rev. A **83**, 031603(R) (2011).

[47] G. Morpurgo, L. Sanchez-Palencia, and T. Giamarchi, Figure data for article "Localization Transition for Interacting Quantum Particles in Colored-Noise Disorder," Zenodo, 10.5281/zenodo.18621366 (2026).

Supplementary material for "Localization Transition for Interacting Quantum Particles in Colored-Noise Disorder"

Giacomo Morpurgo,[1] Laurent Sanchez-Palencia,[2] and Thierry Giamarchi[1]

[1]*Department of Quantum Matter Physics, University of Geneva, 1205 Geneva, Switzerland*
[2]*CPHT, CNRS, Ecole Polytechnique, IP Paris, F-91128 Palaiseau, France*

(Dated: February 11, 2026)

Appendix A: Uncorrelated Gaussian disorder, speckle disorder, and Gaussian Coloured disorder

As a reminder and to ease the comparison between the different disorder distributions which are mentioned in the main text, we detail them a bit more in this section. The average over the configurations of the disorder of an observable $O(W)$, which a priori depends on the disorder configuration W, is denoted by $\overline{O}$ and is the result of the following expression :

$$\overline{O} = \frac{\int dW P(W) O(W)}{\int dW P(W)} \tag{A1}$$

where $P(W)$ is the probability of a given realization of the disorder configuration W and we integrate on all possible disorder configurations W.

a. Uncorrelated Gaussian disorder The disorder distribution which is used as a comparison benchmark through all of the letter is an uncorrelated disorder arising from a Gaussian distribution. A given realization of the disorder V is then drawn from the following probability distribution :

$$P(V) = e^{-\frac{1}{2D}\int dx V(x)^2} = e^{-\frac{1}{2D\Omega}\sum_k V_k V_k^*} \tag{A2}$$

Its correlations are then given by

$$\overline{V(x)V(y)} = D\delta(x-y) \tag{A3}$$

$$\overline{V_k V_{-k'}} = D\Omega\delta_{k,k'} \tag{A4}$$

b. Speckle disorder On the other hand, speckle disorder (SD), which is the main focus of this letter is instead correlated spatially, with correlation functions:

$$\overline{W(x)W(y)} = \frac{W_0^2 k_c}{2\pi}\left(1 + \frac{\sin^2\left((x-y)\frac{k_c}{2}\right)}{\left((x-y)\frac{k_c}{2}\right)^2}\right) \tag{A5}$$

$$\overline{W_k W_{-k'}} = W_0^2\left(1 - \frac{|k|}{k_c}\right)\theta(k_c - |k|)\,\Omega\,\delta_{k,k'} \tag{A6}$$

in real and momentum spaces, respectively.

As can be seen in Eq. (A5), the correlations of this disorder are translation invariant in real space. This leads to the nice property of the correlations that they are diagonal in k-space, but with a coefficient depending on k and which is 0 above a certain k_c. This disorder potential originates from a complex random electric field $\mathscr{E}$. Both real and imaginary parts of its Fourier components $\mathscr{E}_k$ for $|k| < \frac{k_c}{2}$ are random variables originating from a Gaussian distribution $P(\mathrm{Re/Im}(\mathscr{E}_k)) = \frac{1}{\sqrt{2\pi\sigma}} e^{-\frac{1}{2}\frac{\mathrm{Re/Im}(\mathscr{E}_k)^2}{\sigma^2}}$ with variance $\sigma = \left(\frac{\Omega W_0}{|C|}\right)^{1/2}\left(\frac{\pi}{2k_c}\right)^{1/4}$. The factor $\sqrt{\Omega}$ comes when we consider $P(\mathscr{E})$ in its entirety in Fourier space. The potential $W(x)$ felt by the atoms is then given by :

$$W(x) = C\overline{\langle|\mathscr{E}|^2\rangle}\left(\frac{|\mathscr{E}(x)|^2}{\overline{\langle|\mathscr{E}|^2\rangle}} - 1\right), \tag{A7}$$

where, C is a constant which depends on experimental parameters. We take it to be > 0 for the blue-detuned disorder (BSD) and < 0 for the red detuned one (RSD). The quantity $\overline{\langle|\mathscr{E}|^2\rangle} = \frac{\sigma^2 k_c}{\Omega\pi}$ is the spatial and disorder average of $|\mathscr{E}|^2$. The spatial correlation of $W(x)$ obey then (A5).

c. Gaussian colored disorder (Speckle-like disorder) There exists a Gaussian correlated disorder which has the same second order correlations as the speckle disorder. A given realization of this disorder W_{GCD} is given by the following probability distribution

$$P(W_{\mathrm{GCD}}) = e^{\frac{1}{2}\int dx \int dy \tilde{A}^{-1}(x-y)W_{\mathrm{GCD}}(x)W_{\mathrm{GCD}}(y)} \tag{A8}$$

$$= e^{-\frac{1}{2\Omega}\sum_{|k|<k_c} A_k^{-1} W_{\mathrm{GCD},k}^* W_{\mathrm{GCD},k}} \tag{A9}$$

$$A_k = W_0^2\left(1 - \frac{|k|}{k_c}\right) \tag{A10}$$

$$\tilde{A}(x) = \frac{1}{\Omega}\sum_k e^{ikx} A_k \tag{A11}$$

Since there is no distinction between the SD and the GCD at the two-point correlation level, all the calculations which involve only two-point correlations will be identical for both.

Appendix B: Forward disorder

In the derivation of the RG equations of the system, we neglected the forward disorder, we now comment more on its effects. For one dimensional systems, the effects of forward and backward disorder which arise from a given disorder $W(x)$ are completely decoupled, and we can treat them as being two independent realizations of the disorder : W_b and W_f, which have both the original correlations $\overline{W_{b,k}W_{b,-k}} = \overline{W_{f,k}W_{f,-k}} = \overline{W_k W_{-k}}$. The contribution of W_f can be absorbed in the backward disorder by the following

shift of the field ϕ.

$$\widetilde{\phi} = \phi - \frac{K}{u}\int^x dy\, W_f(y) \tag{B1}$$

This shift of ϕ leads to a new "effective" backward disorder $\widetilde{W_b}$ with correlations containing both backward and forward disorder.

$$\overline{\widetilde{W_b}(x)\widetilde{W_b}^*(y)} = \overline{W_b(x)W_b(y)}\,\overline{e^{i\frac{2K}{u}\int_y^x dy\, W_f(y)}} \tag{B2}$$

After performing the disorder average over W_f, consisting mainly in a completion of the square for the field W_f and performing the spatial integral, we get :

$$\overline{\widetilde{W_b}(x)\widetilde{W_b}^*(y)} = \overline{W_b(x)W_b(y)}\,e^{-2\frac{K^2}{u^2}\frac{W_0^2 k_c}{2\pi}f(x-y)} \tag{B3}$$

with

$$\begin{aligned} f(x-y) = \frac{2}{k_c^2}\big[&-2-2\gamma+2\cos[(x-y)k_c] \\ &+(x-y)k_c\,\mathrm{Si}[(x-y)k_c] \\ &-2\log(|x-y|k_c)+2\mathrm{Ci}(|x-y|k_c)\big] \end{aligned} \tag{B4}$$

where γ is the Euler constant, Si is the sine integral and Ci the cosine integral. $f(x)$ is an even function which for large x behaves linearly as : $f(x) \approx \frac{\pi}{k_c}|x-y|$. The backward correlations can then be written as :

$$\overline{\widetilde{W_b}(x)\widetilde{W_b}^*(y)} = \overline{W_b(x)W_b(y)}\,e^{-\frac{|x-y|}{\xi_f}} \tag{B5}$$

with a characteristic forward disorder length

$$\xi_f = \frac{u^2}{K^2}\frac{1}{W_0^2} \tag{B6}$$

which is reminiscent of the one for the uncorrelated Gaussian disorder $\xi_f = \frac{u^2}{2K^2 D}$. [1].

The backward correlations are then exponentially suppressed with this length ξ_f. If this length is large enough, there is no effect on the correlations at order W_0^2 in the disorder. This is the case in particular for weak disorders, where W_0^2 is small. In this regime, neglecting the forward disorder is completely justified. At higher orders, the forward scattering will modify the correlations of the backward terms, leading to a small Fourier component at $2k_F$ of order W_0^4.

Appendix C: Derivation of the RG equations in the bosonization formalism

For this derivation, we follow the procedure of [2]. We can express the disorder by its Fourier components :

$$W(x) = \frac{1}{\Omega}\sum_k W_k e^{ikx} \tag{C1}$$

where Ω is the volume of the system. The part of the action responsible for the disorder scatterings is then given by :

$$\begin{aligned} S_w = \frac{1}{2\pi u\alpha}\int dx \int_0^\beta d\tau \sum_k \frac{W_k}{\Omega} \\ \times\left[e^{i(k^+x-2\phi(x,\tau))}+e^{i(k^-x-2\phi(x,\tau))}\right] \end{aligned} \tag{C2}$$

where $k^\pm = k \pm 2k_F$, τ the imaginary time, $\beta = \frac{1}{k_B T}$ with k_B Boltzmann constant and T the temperature of the system, which we put to 0. The quantity which we are computing before doing the average on the disorder is :

$$\begin{aligned} &\langle T_\tau e^{i\sqrt{2}\phi(x',\tau')}e^{-i\sqrt{2}\phi(x,\tau)}\rangle \\ &\qquad = \frac{\int \mathscr{D}\phi\, e^{i\sqrt{2}\phi(x',\tau')}e^{-i\sqrt{2}\phi(x,\tau)}e^{-S_0-S_W}}{\int \mathscr{D}\phi\, e^{-S_0-S_W}} \end{aligned} \tag{C3}$$

Performing an expansion of S_W in powers of W_k up to order 2, we get the following expression :

$$\langle T_\tau e^{i\sqrt{2}\phi(x',\tau')}e^{-i\sqrt{2}\phi(x,\tau)}\rangle = I_0 - \frac{1}{2\pi u\alpha}I_1 + \frac{1}{8(\pi u\alpha)^2}I_2 \tag{C4}$$

The ensemble averages that appear in I_n involve now only the action without disorder S_0. They are therefore of the shape [1] :

$$\begin{aligned} &\langle T_\tau e^{ic_1\phi(x_1,\tau_1)}\dots e^{ic_n\phi(x_n,\tau_n)}\rangle_0 \\ &\qquad \approx \begin{cases} e^{-\frac{K}{2}\sum_{i>j}c_i c_j \ln\left(\frac{|r_i-r_j|}{\alpha}\right)} & \sum_i c_i = 0 \\ 0 & \sum_i c_i \neq 0 \end{cases} \end{aligned} \tag{C5}$$

where $r = (x, u\tau)$ and $r^2 = x^2 + u^2\tau^2$ and in the limit where $|r_i - r_j| \gg \alpha$. We will also use the following notation $F(r_i - r_j) = K\ln(|r_i - r_j|/\alpha)$.

With all of this, I_0 is therefore given by :

$$I_0 = \langle T_\tau e^{i\sqrt{2}\phi(x',\tau')}e^{-i\sqrt{2}\phi(x,\tau)}\rangle_0 = e^{-F(r-r')} \tag{C6}$$

I_1 is equal to 0 because of (C5). The interesting term is I_2, which will lead to our RG equations. It reads

$$I_2 = \frac{1}{\Omega^2}\sum_{k_1,k_2} W_{k_1}W_{k_2}\int d^2r_1\int d^2r_2 \cdot\Big\{e^{i(k_1^- x_1+k_2^+x_2)}\Big[\langle e^{i(\sqrt{2}\phi(r)-\sqrt{2}\phi(r')+2\phi(r_1)-2\phi(r_2))}\rangle_0 - \langle e^{i(\sqrt{2}\phi(r)-\sqrt{2}\phi(r')}\rangle_0\langle e^{i(2\phi(r_1)-2\phi(r_2)}\rangle_0\Big] + e^{i(k_1^+x_1+k_2^-x_2)}\Big[\langle e^{i(\sqrt{2}\phi(r)-\sqrt{2}\phi(r')+2\phi(r_2)-2\phi(r_1))}\rangle_0 - \langle e^{i(\sqrt{2}\phi(r)-\sqrt{2}\phi(r')}\rangle_0\langle e^{i(2\phi(r_1)-2\phi(r_2)}\rangle_0\Big]\Big\} \quad \text{(C7)}$$

After evaluating the ensemble average on S_0, performing the average on disorder realizations, which directly corresponds in replacing $W_{k_1}W_{k_2}$ by the expression A6, reorganizing the terms, and doing the following change of coordinates : $R = (r_1+r_2)/2, \widetilde{r} = r_1 - r_2$, we obtain the following expression for I_2 :

$$I_2 = \frac{W_0^2}{\Omega}\sum_k\Big(1-\frac{|k|}{k_c}\Big)\theta(k_c-|k|)\int d^2R\int d^2\widetilde{r}\, e^{-2F(r-r')}e^{-2F(\widetilde{r})}2\cos(k\widetilde{x})e^{-i2k_F\widetilde{x}}\Big[e^{\sqrt{2}\widetilde{r}\cdot\nabla_z F(z)|_{r-R}^{r'-R}}-1\Big] \quad \text{(C8)}$$

To continue, we expand the exponential in the square brackets. The zeroth order cancels out and the first order is equal to 0 by symmetry after the sum on k. The first non-zero term is the second order one, which split into two categories. One containing $\nabla_X^2-\nabla_Y^2$ and another $\nabla_X^2+\nabla_Y^2$. Any crossed terms $\nabla_X\nabla_Y$ that would appear are 0 by parity in $\widetilde{y}$. The first of the two surviving terms $(\nabla_X^2-\nabla_Y^2)$ renormalizes the speed u. However, since the correction will be of order W_0^2, they can be neglected in the RG equations at the order in W_0 that we are deriving. Using $\int d^2R[F(r-R)-F(r'-R)](\nabla_X^2+\nabla_Y^2)[F(r-R)-F(r'-R)] = -4\pi KF(r-r')$, passing in polar coordinates for R and integrating on the angle θ (note that θ goes only from 0 to π, since $u\tau$ is only positive), the second term $(\nabla_X^2+\nabla_Y^2)$ becomes :

$$I_2 = e^{-F(r-r')}KF(r-r')\int d\widetilde{r}\,\widetilde{r}^3e^{-2KF(\widetilde{r})}\frac{1}{\Omega}\sum_k 4\pi^2W_0^2\Big(1-\frac{|k|}{k_c}\Big)\theta(k_c-|k|)[J_0((k+2k_F)\widetilde{r})+J_0((k-2k_F)\widetilde{r})] \quad \text{(C9)}$$

Combining I_0 and I_2, after reexponentiating the term in W_0^2, we can define an effective Luttinger parameter K^{eff}. Using the notation $y = \frac{\alpha W_0}{u}$ as defined in the main text, we obtain the following relation.

$$K^{\text{eff}} = K - \frac{K^2y^2}{2\alpha^4}\int_\alpha^\infty d\widetilde{r}\,\widetilde{r}^3e^{-2KF(\widetilde{r})}\frac{1}{\Omega}\sum_k\Big(1-\frac{|k|}{k_c}\Big)\theta(k_c-|k|)[J_0((k+2k_F)\widetilde{r})+J_0((k-2k_F)\widetilde{r})] \quad \text{(C10)}$$

To get the RG equations, we need to look at a small increase of the cutoff $\alpha\to\alpha'$. K^{eff} being a physical observable, it should not depend on the cutoff. We can then rewrite K^{eff} as :

$$K^{\text{eff}} = K(\alpha') - \frac{K^2y^2}{2\alpha^4}\int_{\alpha+d\alpha}^\infty d\widetilde{r}\,\widetilde{r}^3\Big(\frac{\widetilde{r}}{\alpha}\Big)^{-2K}\frac{1}{\Omega}\sum_k\Big(1-\frac{|k|}{k_c}\Big)\theta(k_c-|k|)[J_0((k+2k_F)\widetilde{r})+J_0((k-2k_F)\widetilde{r})] \quad \text{(C11)}$$

$$K(\alpha') = K(\alpha) - \frac{K^2y^2}{2}\int_\alpha^{\alpha'}\frac{d\widetilde{r}}{\alpha}\Big(\frac{\widetilde{r}}{\alpha}\Big)^{3-2K}\frac{1}{\Omega}\sum_k\Big(1-\frac{|k|}{k_c}\Big)\theta(k_c-|k|)[J_0((k+2k_F)\widetilde{r})+J_0((k-2k_F)\widetilde{r})] \quad \text{(C12)}$$

Taking α' infinitesimally close to α with the following parametrization : $\alpha' = \alpha(l+dl) = \alpha(l)e^{dl}$ in (C12) leads to the RG equation (5) of the main paper :

$$\frac{\partial K}{\partial l} = -\frac{K^2y^2}{2}\frac{1}{\Omega}\sum_k\Big(1-\frac{|k|}{k_c}\Big)\theta(k_c-|k|)\Big[J_0\big((k+2k_F)\alpha(l)\big)+J_0\big((k-2k_F)\alpha(l)\big)\Big] \quad \text{(C13)}$$

To obtain the RG equation for y, one has to look at the last term of (C11), where to recast it as an equation where

all α have become α', we have to define :

$$y^2(\alpha') = y^2(\alpha)\left(\frac{\alpha'}{\alpha}\right)^{4-2K} \tag{C14}$$

which then yields the RG equation for y :

$$\frac{\partial y}{\partial l} = (2-K)y \tag{C15}$$

The last step left is to replace the Bessel functions in (C13) by closed windows of size $1/\alpha(l)$ around $2k_F$: $J_0(k\alpha) \to \theta(1-|k|\alpha)$, we can then perform the sum on the momenta and get the final form of the RG equations.

For the case $k_c > 2k_F$, we have that the sum on the momenta (taking the the limit to the continuum) yields for $\alpha(l)$ large enough (such that $k_c > 2k_F + \frac{1}{\alpha(l)}$) :

$$\frac{1}{2\pi}\left(\int_{-2k_F-\frac{1}{\alpha(l)}}^{-2k_F+\frac{1}{\alpha(l)}} + \int_{2k_F-\frac{1}{\alpha(l)}}^{2k_F+\frac{1}{\alpha(l)}}\right) dk \left(1-\frac{|k|}{k_c}\right) = \frac{4(k_c-2k_F)}{2\pi k_c \alpha(l)} \tag{C16}$$

$$\frac{\partial K}{\partial l} = -\frac{K^2(k_c-2k_F)}{\pi k_c}\frac{y^2}{\alpha(l)} \tag{C17}$$

$$\frac{\partial y}{\partial l} = (2-K)y \tag{C18}$$

By absorbing a factor $\sqrt{\alpha(l)}$ in the definition of $y = \sqrt{\alpha(l)}\tilde{y}$, these equations can be recasted in :

$$\frac{\partial K}{\partial l} = -\frac{K^2(k_c-2k_F)}{\pi k_c}\tilde{y}^2 \tag{C19}$$

$$\frac{\partial \tilde{y}}{\partial l} = \left(\frac{3}{2}-K\right)\tilde{y} \tag{C20}$$

where now no cutoff $\alpha(l)$ appears and it is quite clear that we recover, as in the case of uncorrelated Gaussian disorder, that the transition point separating the relevance from irrelevance of the disorder is at $K = 3/2$.

For the case $k_c = 2k_F$, the sum on the momenta yields a different result. Here it is crucial that while one of the two bounds of the integral on k is dictated by the "RG window" as before, the other is now fixed by $\pm k_c$ and does not depend on $\alpha(l)$.

$$\frac{1}{2\pi}\left(\int_{-k_c}^{-k_c+\frac{1}{\alpha(l)}} + \int_{k_c-\frac{1}{\alpha(l)}}^{k_c}\right) dk \left(1-\frac{|k|}{k_c}\right) = \frac{1}{2\pi k_c \alpha^2(l)} \tag{C21}$$

This leads to the following RG equations :

$$\frac{\partial K}{\partial l} = -\frac{K^2}{4\pi k_c}\frac{y^2}{\alpha^2(l)} \tag{C22}$$

$$\frac{\partial y}{\partial l} = (2-K)y \tag{C23}$$

and by absorbing a factor $\alpha(l)$ in the definition of $y = \alpha(l)\tilde{y}$, these equations can be recasted in :

$$\frac{\partial K}{\partial l} = -\frac{K^2}{4\pi k_c}\tilde{y}^2 \tag{C24}$$

$$\frac{\partial \tilde{y}}{\partial l} = (1-K)\tilde{y} \tag{C25}$$

The advantage of this writing is that again there is no $\alpha(l)$ in the equations. From these expressions, it naturally follows that the transition point occurs at $K = 1$.

The generalization to correlations behaving as $(1-|k|/k_c)^\nu$ is obtained by keeping track of the ν exponent and adding it in (C13). In the case $k_c > 2k_F$, the sum on k in (C16) gives still a result proportional to $\frac{1}{\alpha(l)}$ and we recover the same K^* as for the uncorrelated Gaussian disorder. On the other hand, for the case $k_c = 2k_F$, the sum on k in (C21) yields a result which depends on ν : $\frac{1}{2\pi k_c^\nu}\frac{2}{1+\nu}\frac{1}{\alpha^{\nu+1}}$. This change means that after redefining $y = \alpha^{\frac{\nu+1}{2}}\tilde{y}$ in order to have RG equations that do not depend explicitly on the cutoff, we find the following equations :

$$\frac{\partial K}{\partial l} = -\frac{K^2}{4\pi}\frac{2}{(1+\nu)k_c^\nu}\tilde{y}^2 \tag{C26}$$

$$\frac{\partial \tilde{y}}{\partial l} = \left(\frac{3-\nu}{2}-K\right)\tilde{y} \tag{C27}$$

We can finally conclude that for this problem $K^* = \frac{3-\nu}{2}$.

Appendix D: Derivation of the RG equations for interacting fermions perturbative in interactions

To get the renormalizations equations perturbatively in the interaction g and disorder W_0^2, we have to compute the following correlation functions, which correspond respectively to the backward scattering and interaction diagram.

For the backward scattering, we have to compute the following expression

$$\left\langle T_\tau \left[c_{-r}(k+q,\tau_4)c_r(k'-q,\tau_3) \right.\right. \\ \left.\left. c^\dagger_{-r}(k',\tau_2)c^\dagger_r(k,\tau_1)e^{-\int_0^\beta d\tau' H_{g,W_0}}\right]\right\rangle_{H_0} \tag{D1}$$

As in the main text, r denotes the right and left movers, $\varepsilon_r = \pm 1$ correspondingly. Here H_0 is just the free Hamiltonian without disorder or interaction, and H_{g,W_0} contains the interaction and backward scattering terms of equation (9) of the main text.

Instead, for the interaction, we have to compute the following expression :

$$\left\langle T_\tau \left[c_r(k+q,\tau_4)c_{-r}(k'-q,\tau_3) \right.\right. \\ \left.\left. c^\dagger_{-r}(k',\tau_2)c^\dagger_r(k,\tau_1)e^{-\int_0^\beta d\tau' H_{g,W_0}}\right]\right\rangle_{H_0} \tag{D2}$$

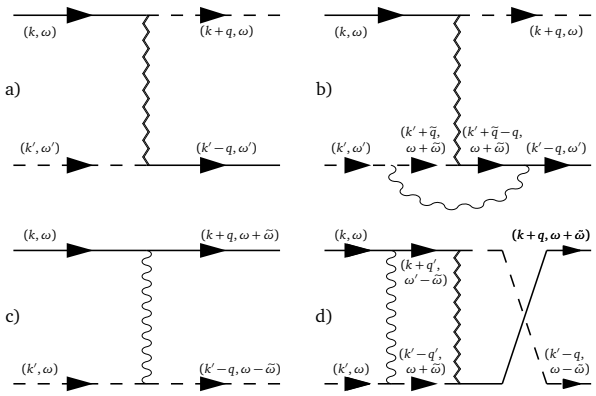

FIG. 1. Diagrams contributing to the renormalization of interactions and disorder up to order two in g and W_0^2. The solid (resp. dashed) lines denote right (resp. left) movers. The wiggly line is the interaction g, while the zig-zag line indicate the averaged disorder line. The frequencies written are Matsubara frequencies. The panels a) and b) show, respectively, first and second order disorder backscattering diagrams. Frequencies are conserved separately on the top and bottom lines for these diagrams since the disorder is time independent. The panels c) and d), respectively, show first and second orders of the interaction diagram. In such a diagram, frequency can be exchanged between the top and bottom lines.

We perform an expansion of the exponential up to 2nd order in g, W_0^2 and apply Wick's theorem to the creation/annihilation operators since H_0 is quadratic. Each pair of creation/annihilation can be written as a free electron Green's function/propagator in imaginary time:

$$G_{o,r}(k,\tau) = -\langle T_\tau c_r(k,\tau) c_r^\dagger(k,0)\rangle \tag{D3}$$

The Green's function admits a Matsubara frequency representation $G(k,\tau) = \frac{1}{\beta}\sum_{i\omega_n} G(k,i\omega_n)e^{-i\omega_n\tau}$, with $\omega_n = (2n+1)\pi/\beta$ [3]. For simplicity of notation, we drop the index n from ω_n in the following. The Matsubara free electron propagator has the shape :

$$G_{o,r}(k,\omega) = \frac{1}{i\omega - v_F(\varepsilon_r k - k_F)} \tag{D4}$$

The first order term of (D1) can now be related to the diagram shown in Figure 1.a) , while the first order term of Eq. (D2) can now be related to the diagram shown in Figure 1.c). Each line is the free electron propagator (continuous lines are right movers and dashed lines are left movers). The zig-zag line denotes the backscattering process, which carries a momentum q but no frequency and has a weight given by $\overline{W_q W_{-q}} = A(q)\theta(k_c - |q|)$. The wiggly line denotes the interaction process, which carries a momentum q, a frequency $\tilde{\omega}$ and has a weight of g.

The second order in the expansion of (D1) leads in particular to the diagram shown in Figure 1.b), which renormalizes the diagram in Figure 1.a), while for (D2) we find the diagram of Figure 1.d) which renormalizes the one in Figure 1.c). We then have to perform the integrals/sums over the internal degrees of freedom [3] of Figure 1.b) (and Figure 1.d)) to find the renormalization of $A(q)\theta(k_c - |q|)$ (and g). For the diagram in Figure 1.b), the variables on the external legs can expressed as : $k = k_F + \delta k$, with δk small since this leg corresponds to a right mover and $k' = -k_F - \delta k'$ with $\delta k'$ small, since this leg corresponds to a left mover. The result is independent of the external frequencies and diverges logarithmically in the cutoff on the momenta Λ as : $-\frac{gA(q)\theta(k_c-|q|)}{4\pi v_F}\ln\left[\frac{4\Lambda^2}{(q-2k_F)^2}\right]$. For the diagram in Fig. 1.d), which renormalizes the interaction term g, we make the same choice of k and k' as before. To extract the main divergence, there is a smart choice of the external frequencies which simplifies the expressions [4]. We thus take $\omega = -\frac{1}{2}\tilde{\omega}$ and $\omega' = \frac{3}{2}\tilde{\omega}$. We find that the leading divergence for $q = 0$ is also logarithmic in the cutoff and is given by : $-\frac{gW_0^2}{4\pi k_c v_F^2}\ln\left(\frac{v_F^2\Lambda^2}{\tilde{\omega}^2/4}\right)$.

There are two more diagrams of order g^2, which could be relevant in the interaction renormalization. The first has two parallel interaction lines and the second has crossed interaction lines. However, their divergences in Λ cancel exactly and they do not intervene in our RG. We therefore find an effective interaction g^{eff} and an effective disorder strength $W_0^{2\,\text{eff}}$ given by :

$$g^{\text{eff}} = g - \frac{gW_0^2}{4\pi k_c v_F^2}\ln\left(\frac{4v_F^2\Lambda^2}{\tilde{\omega}^2}\right) \tag{D5}$$

$$W_0^{2\,\text{eff}}\theta(k_c - |q|) = W_0^2\theta(k_c - |q|) - \frac{gW_0^2}{4\pi k_c v_F^2}\ln\left[\frac{4\Lambda^2}{(q-2k_F)^2}\right]\theta(k_c - |q|) \tag{D6}$$

The final step to get the RG equations is then to keep the effective variables constant when we decrease the cutoff $\Lambda(l+dl) = \Lambda(l)e^{-dl}$. We then obtain the RG equations (10) and (11) of the main text.

Appendix E: Numerical generation of the disorder

To find the localization length of the system, we need to generate the disorder following different disorder distributions. For the Gaussian colored disorder, since the disorder correlations are translation invariant, we generate first each Fourier component of the disorder W_q with the probability distribution given by (A8). Once we have all of the W_k we can Fourier transform them back to have the disorder $W(x)$ in real space. Note that $W(x)$ is real, therefore there is a condition on its Fourier component $W_k = W_{-k}^*$.

For the real speckle disorder (both blue and red), we start by generating the complex Fourier components of the electric field $\mathscr{E}_k$ as defined in section A. We then Fourier transform it to have the electric field in space and compute $W(x)$ using (A7). We took the numerical values $C = 1$, which generates a BSD. Because of the particle-hole ($d_i^\dagger = (-1)^i c_i$) symmetry of the Hamiltonian when also changing the sign of W_i, we could find the RSD properties by looking at $k_{\text{E,RSD}} = \pi - k_{\text{E,BSD}}$.

Appendix F: Average over the disorder of the IPR

For each Hamiltonian generated, we compute the IPR as a function of the energy. Since we have a finite number of sites (10000), we have a finite number of eigenvalues of the energy. To perform the average over the disorder, we have to bin our energy space. We do this by selecting the minimal and maximal eigen energies among all 1000 disorder realizations. We then separate this interval in 400 bins of same size ΔE. For each realization i of disorder, we compute the IPR associated to a given bin $\mathrm{IPR}^i_{E,E+\Delta E}$ by averaging over all eigenstates which fall in the corresponding energy range $\mathrm{IPR}^i_{E,E+\Delta E} = 1/N^i_{E,E+\Delta E} \sum_{E<E_n<E+\Delta E} \mathrm{IPR}^i(E_n)$. Finally, we average this IPR for the same bin over all realizations N_{real} : $\mathrm{IPR}_{E,E+\Delta E} = \frac{1}{N_{\mathrm{real}}} \sum_i \mathrm{IPR}^i_{E,E+\Delta E}$.

Appendix G: Localization length when $k_c < 2k_F$

For $k_c < 2k_F$, we find that ξ is of the order of the system size, which suggests that there is no localization. This is consistent with the results of [5], which showed that the second order Lyapunov exponent vanishes and only higher order can give a finite localization length. Such a length is too large for our numerical calculation to capture it. This shows clearly that although higher order harmonics of the disorder formally still lead to localization, the system is practically not localized in that case.

Appendix H: Localization length when $k_c > 2k_F$

Using the same procedure as in the main paper, we look at the localization length scaling of the strength of the disorder, for $k_F = 3k_c/8$, which is an example of the regime $k_c > 2k_F$, where there are finite components of backscattering. As shown in Figure 2, we recover the D^{-1} scaling associated to the uncorrelated Gaussian disorder, and this for the CGD, BSD and RSD. We also see here that we reach the strong disorder regime where the localization length does not follow the scaling anymore.

Appendix I: Effects of the system size on the localization length

To ensure our interpretation of the saturation of $\xi(D)$ for low disorder strengths, we provide here a study of its dependence for various number of sites N in the case of GCD. First, in our procedure, we have to divide evenly the energy spectrum in order to perform the disorder average. The number of bins varies as a function of the system size and Table I contains the values used.

In Figure 3, we see that the saturation at low-disorder is dependent on the number sites ($\xi_{\mathrm{sat}} \approx N_{\mathrm{sites}}/3$) and, as we increase the system size, converges on a $D^{-3/2}$ power-law when the "real" localization length becomes smaller than the saturated localization length.

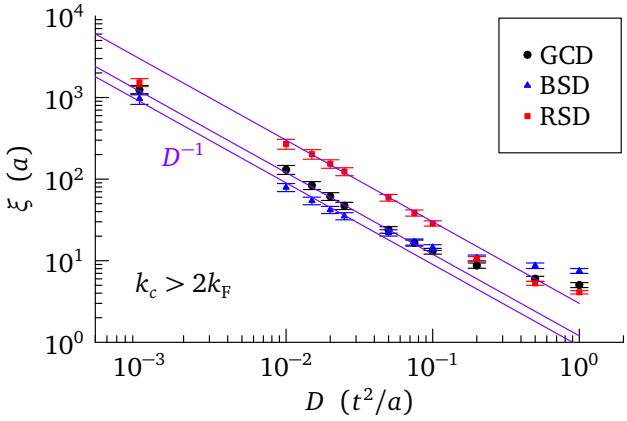

FIG. 2. Localization length ξ as a function of disorder strength D for eigenstates at momentum $k_F = 3k_c/8$ of a noninteracting system with GCG (black circles), BSD (blue triangles) and RSD (red squares). The error bars indicate the standard deviation coming from the different disorder realizations. The localization length shows the usual scaling D^{-1} of the uncorrelated disorder. The lines plotted are guides to the eye.

N	100	500	1000	2000	5000	10000
Number of bins	10	50	100	200	200	400

TABLE I. Table containing the number of bins used to divide evenly the energy spectrum for each system size N before the average on the disorder realizations.

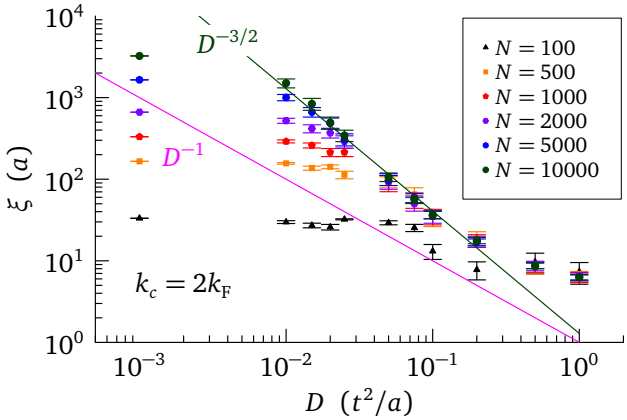

FIG. 3. Localization length ξ as a function of disorder strength D for eigenstates at momentum $k_F = k_c/2$ of a noninteracting system with GCG for six different sizes N of the system. The error bars indicate the standard deviation coming from the different disorder realizations.

Disorder type	Exponent	Fitting range
RSD	1.4 ± 0.1	$D \in [0.02, 0.5]$
GCD	1.6 ± 0.1	$D \in [0.01, 0.1]$
BSD	1.5 ± 0.3	$D \in [0.01, 0.05]$

TABLE II. Table containing the fits of the exponents and the fitting ranges for the three disorders at $k_c = 2k_F$ with $N = 10000$.

Appendix J: Fitting the power-law exponent of the localization length scaling

While in Figure 4 of the main text we showed guide to the eyes of a power-law decay of 3/2, fitting a generic power-law to the $N = 10000$ results yields the exponents in the three cases studied presented in Table II. For each type of disorder, the fitting range was given on the lower bound by the saturation of ξ to ξ_{sat} and on the upper bound by the system exiting the weak disorder phase, as given by the $k_c > 2k_F$ case. The exponents found are consistent with a scaling of $D^{-3/2}$.

[1] T. Giamarchi, *Quantum Physics in One Dimension*, International series of monographs on physics, Vol. 121 (Oxford University Press, Oxford, 2004).

[2] J. Vidal, D. Mouhanna, and T. Giamarchi, Interacting fermions in self-similar potentials, Phys. Rev. B **65**, 014201 (2001).

[3] G. Mahan, *Many-Particle Physics* (Springer New York, 2000).

[4] J. Sólyom, The Fermi gas model of one-dimensional conductors, Adv. Phys. **28**, 201 (1979).

[5] P. Lugan, A. Aspect, L. Sanchez-Palencia, D. Delande, B. Grémaud, C. A. Müller, and C. Miniatura, One-dimensional Anderson localization in certain correlated random potentials, Phys. Rev. A **80**, 023605 (2009).